

## **ENSO modulated cyclogenesis over the Bay of Bengal**

Clifford S. Felton<sup>1</sup>, Bulusu Subrahmanyam<sup>1,2</sup>, V.S.N. Murty<sup>3</sup>

1. Marine Science Program, University of South Carolina, Columbia, SC 29208.
2. Department of Earth and Ocean Sciences, University of South Carolina, Columbia, SC 29208.
3. Council of Scientific and Industrial Research (CSIR) - National Institute of Oceanography (NIO) Regional Center, Visakhapatnam 530 017, India.

### **Abstract**

The role of El Niño Southern Oscillation (ENSO) on the modulation of tropical cyclone activity over the Bay of Bengal (BoB) for the 1979-2011 period is examined. It is shown that Niño3.4 sea surface temperature (SST) anomalies are negatively correlated with the BoB tropical cyclone activity to a statistically significant percentage by a lead-time of five months. Composites of 10-meter zonal winds exhibit greater variance during La Niña events favoring the development of low-level cyclonic vorticity. Low vertical wind shear over the central and northern BoB also aids the development of tropical cyclones during La Niña events. Increased relative humidity is the result of enhanced moisture transport and higher precipitable water under La Niña conditions. Furthermore, storm relative composites of relative humidity show stronger moisture pulses over the BoB during La Niña. The enhanced moisture associated with tropical cyclogenesis likely aids the development and strengthening of the systems. ENSO forces modulations in oceanic conditions as well. The observed negative (positive) SST anomalies during La Niña (El Niño) could be seen as the result of increased (decreased) net heat flux across the sea surface. Tropical cyclone activity varies between El Niño and La Niña due to anomalous wind and moisture patterns during each ENSO phase.

<sup>1</sup> *Corresponding author address:* Clifford S. Felton, Marine Science Program, University of South Carolina, 701 Sumter Street, EWS 617, Columbia SC 29208.  
Email: [cfelton@geol.sc.edu](mailto:cfelton@geol.sc.edu)

## 1. Introduction

Tropical cyclones (TCs) are among the most destructive natural events that form in the world's oceans. Characterized by strong winds, heavy rainfall, and destructive storm surge, TCs cause considerable economic and societal damage along coastlines as well as further inland. The Bay of Bengal (BoB) is one of the more vulnerable regions to these effects due to its low-lying topography and population density along the coastline. The BoB is a semi-enclosed ocean-basin, located in the Northern Indian Ocean that exhibits a unique bimodal seasonal distribution of tropical cyclone activity (Fig. 1) due to unfavorable environmental conditions during the monsoon season (Li et al. 2013). Peak TC activity occurs during October-December (post-monsoon) with a secondary maximum during March-May (pre-monsoon). In order to forecast TCs accurately, it is necessary to understand the environmental factors that influence TCs in this region.

Oceanic and atmospheric conditions are important for the development, strengthening and movement (track) of tropical cyclones across the BoB. The seasonal and intraseasonal transitions play an important role in altering TC environment in the BoB (Goswami et al. 2003; Kikuchi and Wang 2010; Yanase et al. 2012). Recent studies (Kikuchi et al. 2009; Lin et al. 2009; McPhaden et al. 2009; Maneesha et al. 2012) have highlighted the importance of oceanic thermal structure on the intensification of very severe cyclonic storm Nargis that devastated Myanmar in 2008. The study by Singh et al. (2000) has shown that tropical cyclone (TC) activity during the seasonal peaks of November and May is trending upwards and exhibits a prominent El Niño-Southern Oscillation (ENSO)-scale oscillation of 2-5 years over the BoB.

The ENSO is well known to be one of the primary climatic features causing global alterations in atmospheric and oceanic patterns. The two extremes associated with the ENSO, termed as El Niño and La Niña events, describe the SST anomalies (SSTAs) in the central Pacific Ocean (Bjerknes, 1969). The ENSO signal exhibits similar seasonal progressions, with SSTAs beginning to emerge in the central Pacific Ocean during April-June, peaking later during November-January. Though research on the affect of the ENSO on tropical cyclones in the Atlantic and Pacific Oceans is well documented, far less research has been conducted over the BoB. Alterations in SST and relative vorticity during El Niño facilitate increased cyclogenesis during July-August of El Niño years in the BoB (Singh et al. 2001). Camargo et al. (2007) found that vertical wind shear played the primary role in altering tropical cyclogenesis locations in the BoB during ENSO events after examining the parameters that compose a genesis potential index developed by Emanuel and Nolan (2004). Recent research by Girishkumar and

Ravichandran (2012) (from here onwards GR (2012)) indicates that ENSO influences tropical cyclone environment over the BoB during October-December by forcing anomalous patterns in convection, low-level cyclonic vorticity, and tropical cyclone heat potential (TCHP). The present study looks beyond these findings by investigating the large-scale dynamics forcing these and other important environmental modulations.

Research on the impacts of the ENSO on tropical cyclones over the BoB is limited compared to other ocean basins. In this paper, we focus on the period from 1979-2011 to investigate the ENSO forced modulations in environmental conditions over the BoB. In addition, we diagnose the impacts on tropical cyclone activity. This paper is organized as follows: Section 2 describes the data set and methods used for the study. An overview of TC activity over the BoB during ENSO events is presented in section 3. Section 4 investigates the impact of the ENSO on TC environment in the BoB. A summary and discussion of the findings are presented in section 5.

## **2. Data and Methods**

Northern Indian Ocean TC tracks are obtained from the U.S. Navy's Joint Typhoon Warning Center's (JTWC) best track data site (<http://www.usno.navy.mil/JTWC/>). The best track data is filtered to remove storms that 1) formed over the Arabian Sea, 2) formed over land, and 3) did not track into the BoB. The remaining storms that reached minimum wind speeds of 20 knots (kt) are only included. For this study tropical cyclogenesis (depression formation) occurs at this minimum value (20 kt) since the JTWC records maximum wind observations at 5 kt increments with most storms being identified when a minimum wind speed of 20 kt was achieved. While the India Meteorological Department (IMD) defines a tropical cyclone when the wind speeds exceed 34 kt, the JTWC database utilizes 35 kt. For this reason wind speeds  $\geq 35$  kt are used as the threshold value for tropical cyclones while 20 - 34 kt is used for depressions throughout the analysis.

Monthly average SST data for the Niño3.4 region ( $5^{\circ}\text{N}$ - $5^{\circ}\text{S}$ ,  $120^{\circ}\text{W}$ - $170^{\circ}\text{W}$ ) is obtained from the National Oceanic and Atmospheric Administration's (NOAA) Climatic Prediction Center (<http://www.cpc.ncep.noaa.gov/>) for the 1979-2011 period in order to calculate the Niño3.4 index for the study. Seasons are termed as "El Niño" or "La Niña" if the 5-month running mean SSTAs exceed a threshold value of  $\pm 0.4^{\circ}\text{C}$  for 6 months or more consecutive months as defined by Trenberth (1997).

Daily and monthly atmospheric analysis estimates (wind and relative humidity) from the National Center for Environmental Prediction Department of Energy Intercomparison Model Project reanalysis 2

(NCEP-DOE R-2 or NCEP-2) for the period 1979-2011 are used in this study. The horizontal resolution of the product is  $2.5^\circ \times 2.5^\circ$  grid with 17 levels in the vertical (Kanamitsu et al., 2002). Composites are created for El Niño and La Niña events during the post-monsoon season using the NCEP-2 data. A storm relative reference frame is adopted to examine the variability of atmospheric parameters before, during and after the formation of tropical systems. In order to remove the possible influence of the tropical cyclone on the spatial fields, daily estimates are smoothed following similar methods as in Kurihara et al. (1990). This method removes all wavelengths less than  $7.5^\circ$ . To reduce the possible impact of a tropical cyclone on the temporal fields, a 15-day filter is also applied. 10-meter wind estimates are linearly interpolated onto a  $2^\circ \times 2^\circ$  grid from the original Gaussian grid in order to perform the filtering method. Comparisons between high-pass filtered and smoothed linearly interpolated 10-meter wind estimates yielded similar results. All atmospheric anomalies are based off of the 33-year October through December means (1979-2011).

Vertically integrated moisture transport ( $\mathbf{Q}$ ) and precipitable water ( $W$ ) are used to diagnose moisture content over the BoB during ENSO events. If the atmosphere is assumed to be in hydrostatic balance,  $p$  can be expressed as a vertical coordinate. Precipitable water ( $W$ ,  $\text{kg m}^{-2}$ ) in the air column can then be expressed by

$$W = g^{-1} \int_{ps}^{pt} q dp, \quad (1)$$

where  $g$  is the acceleration due to gravity ( $9.81 \text{ m s}^{-2}$ ),  $q$  is the specific humidity ( $\text{kg kg}^{-1}$ ),  $ps$  is pressure at the surface (Pa) and  $pt$  the pressure at the top of the atmosphere (Pa). The total moisture transport  $\mathbf{Q}$  ( $\text{kg m}^{-1} \text{ s}^{-1}$ ) above the Earth's surface can be written as

$$\mathbf{Q} = g^{-1} \int_{ps}^{pt} q \mathbf{V} dp, \quad (2)$$

where  $\mathbf{V}$  represents the total wind vector ( $\text{m s}^{-1}$ ),  $u$  (positive eastward) and  $v$  (positive northward). Vertical integrations were performed using the trapezoidal rule from lowest model level,  $ps$  (1000 hPa), to the highest level where humidity is available,  $pt$  (300 hPa). Mixing ratio is computed from vertical profiles of temperature and relative humidity from the NCEP-2 reanalysis following methods from Bolton (1980).

Monthly outgoing long wave radiation (OLR) and Global Precipitation Climate Project (GPCP) precipitation data are used as proxies for vertical motion and convective activity during each ENSO regime. The NOAA/OAR/ESRL PSD, Boulder, Colorado, USA provided both datasets from their web site at <http://www.esrl.noaa.gov/psd/>. Each product has a horizontal resolution of  $2.5^\circ \times 2.5^\circ$ .

Simple Ocean Data Assimilation (SODA) reanalysis is used to discern the sea surface temperatures patterns (SST) during each respective ENSO phase. In this study, we used SODA version 2.2.4 reanalysis output from 1979-2008 (Giese and Ray, 2011). Anomalies are based off the October through December means from 1979-2008. This version of SODA combines an ocean model based on the Parallel Ocean Program (POP) version 2.0.1 numerics (Smith et al., 1992) with the assimilation of hydrographic temperature and salinity data. The model outputs are mapped onto a uniform  $0.5^\circ \times 0.5^\circ$  horizontal grid with 40 levels in the vertical. The use of data assimilation allows sparse observational datasets to be optimally merged with high performance ocean models to provide an estimation of ocean variables.

### 3. Climatology of Tropical Cyclones during ENSO

#### *a. Seasonal Tropical Cyclone Activity*

Before examining the impact of the ENSO on tropical cyclone environment, a brief climatology of TC activity over the BoB is presented. In order to take into account the strength, number and duration of the tropical cyclones for analysis, accumulated cyclone energy (ACE) is calculated using the formula (3):

$$ACE = 10^{-4} \sum v_{max}^2, \quad (3)$$

where  $v_{max}$  is the sustained maximum wind speed in knots from the 6-hourly JTWC observations. The values are summed over the life of each tropical system when wind speeds are in excess of 35 knots. Seasonal tropical cyclone occurrences and ACE for each month over the study period (1979-2011) are shown in Fig 1. Two seasonal peaks can be seen in May and October when atmospheric and oceanic conditions are most favorable over the BoB (Li et al. 2013). During the period from 1979-2011, a total of 118 tropical systems formed over the BoB with 74 occurring from October through December (post-monsoon) and 25 from March through May (pre-monsoon). Of the 74 storms that formed during the post-monsoon season, 31 developed during La Niña events while only 16 occurred during El Niño events (Table 1). Comparing only developing depressions (i.e. TCs with maximum speeds  $> 35$  kt), TCs

during La Niña are twice as prevalent when compared to El Niño years. The post-monsoon tropical cyclone genesis locations and tracks during El Niño (Fig 2a) and La Niña (Fig 2b) events also show differing trends. Genesis locations and tracks during El Niño events trend more westward (85.2°E) while during La Niña years there is a significant ( $p < 0.01$ ,  $t$  test) eastward (90.6°E) shift in genesis sites with wider varying track and landfall patterns. Pre-monsoon TC genesis and tracks are shown in Fig 3. Tracks are not separated by ENSO phase due to the low number of ENSO events (2 El Niño, 4 La Niña respectively) extending into the pre-monsoon season. Landfalls are concentrated along the northern and western BoB due to the prevailing upper wind patterns prior to the monsoon season.

### ***b. Post-monsoon TC Activity***

To determine the connection between ENSO and TC activity over the BoB, a series of statistical analyses are performed. Correlation tests between October–December averaged ACE and monthly Niño3.4 SSTA can be seen in Table 2. Correlations during all months were negative with the highest and most significant occurring from May (-0.38,  $p < 0.05$ ) increasing until December (-0.66,  $p < 0.01$ ). These results agree with the findings of GR (2012) that ACE is negatively correlated during October – December and that tropical cyclone activity during La Niña (El Niño) years is higher (lower). Increasing correlations found from May to December are the result of the lead-lag relationship between ENSO and TC activity over the BoB. The development of an ENSO event typically leads post-monsoon TC activity, which explains why correlations increase towards the start of the post-monsoon TC season. These results show that the boreal summer Niño3.4 SSTAs are significantly correlated with ACE during the post-monsoon season indicating that the Niño3.4 index can serve as a proxy for TC activity in the months prior to a mature ENSO event.

### ***c. Pre-monsoon TC Activity***

Due to the seasonal locking of ENSO, events typically do not persist into the pre-monsoon tropical cyclone season over the BoB. However, these months represent a time when ENSO events have ceased a few months prior or may commence in the upcoming months. To test if a lagged or preceding ENSO signal is present, correlations are run between the Niño3.4 SSTAs and ACE from March to May (Table 3). Correlations were low and all relationships failed to reach statistically significant values indicating that an ENSO signal is not present in March – May ACE totals. Correlations are poor during this time since the ENSO typically peaks around December and the signal weakens from March through May when the northward-propagating intraseasonal oscillations dominate the environment over the BoB (Li

et al. 2013). Since the correlations between ACE and Niño3.4 SSTAs during the pre-monsoon season are poor, the rest of the paper will focus on the post-monsoon time frame.

#### **4. Modulation of BoB environment during ENSO**

To determine the ENSO forced modulations over the BoB, an analysis of the environmental factors that contribute to convection and tropical cyclones is performed. Relative humidity, vorticity, wind shear and SSTs have been shown to be the major environmental parameters that impact seasonal tropical cyclone formation over the BoB (Singh et al. 2001; Kikuchi and Wang 2010; Yu and McPhaden 2011; Yanase et al. 2012). As such, our analyses focus on these parameters. Low-level winds are important for TC development since they can transport moisture and enhance cyclonic vorticity. The low-level jet over the Indo-Chinese peninsula is weaker El Niño (Fig. 4a) while during La Niña, the jet is stronger leading to enhanced convergence (Fig. 4b). Wind anomalies reverse direction along the southern BoB between ENSO phases due variations in convective activity, which will be examined later. This results in anomalous anti-cyclonic vorticity over the central and western BoB during El Niño events (Fig. 4c) and anomalous cyclonic vorticity during La Niña (Fig. 4d). The increase in low-level cyclonic vorticity favors TC development during La Niña comparatively.

Large-scale wind patterns force ascent over the BoB during La Niña events as well. OLR (Fig. 5a) and GPCP (Fig. 5b) anomalies indicate ENSO altered convective and precipitation patterns due to the ENSO. During El Niño, convective activity over the eastern BoB and Gulf of Thailand is reduced (Fig. 5a). Convection in this region is typically sustained by the heat and moisture fluxes from high SSTs and the rising limb of the Walker Cell. During El Niño, the rising limb of the Walker Cell, and associated convection, moves eastward in response to enhanced SSTs over the Central Pacific. The presence of positive OLR and negative precipitation anomalies indicate that sinking motion is enhanced during El Niño events due to this eastward shift. Conversely, the patterns during La Niña are reversed. Lower OLR values (enhanced convection) and higher precipitation are present over the eastern BoB and Indo-Chinese peninsula are due to the enhancement of the Walker cell's rising limb over the western Pacific and Indonesia (Fig. 5b). The increase in convective activity and precipitation act to precondition the atmosphere for tropical cyclone development through enhanced moisture and lift.

Westerly winds along the equator south of the BoB are also important for the generation of westerly wind bursts which generate enhanced cyclonic vorticity in the lower levels of the atmosphere (Kikuchi et al. 2009). The cyclonic rotation in the lower levels acts to remove the low level stable air mass that forms below intense convection due to latent cooling from precipitation outflow (Gray 1998). This

results in higher pressure in the lower level of the atmosphere that weakens convergence under the convective system. The presence of background cyclonic vorticity acts to remove the stable air mass and provide convergence for convective systems favoring development. Once the low level stable air is removed, air-sea fluxes can begin to initiate, leading to tropical cyclone development if environmental conditions are favorable. Over the BoB, zonal 10-m winds exhibit more variance during La Niña (Fig. 6). Surface winds in equatorial regions are largely driven by pressure differentials due to the weak Coriolis force. The presence of enhanced convective activity over the eastern BoB and Indian Ocean creates a favorable environment for these wind bursts to occur by mass conservation arguments. As the post-monsoon season progresses surface winds begin to blow from the northeast. With the presence of strong westerly winds along the equator this creates low-level cyclonic flow. Furthermore, winds over Thailand and the Malay Peninsula also exhibit more variance, favoring the development of low-level cyclonic flow. Stronger surface winds can also facilitate moisture flux into the atmosphere, which will be examined later.

Wind shear is another important environmental parameter that impacts tropical cyclogenesis (Gray, 1968). The highest environmental wind shear during TC genesis for all storms over the study period was  $26 \text{ m s}^{-1}$ . Climatological wind shear over the entire BoB remains below this value under both El Niño and La Niña regimes. Both ENSO phases exhibit wind shear minima over the central BoB where tropical cyclones form, similar to climatological conditions (Fig. 7a). However, shear anomalies reverse sign over the northern and southern BoB between El Niño (Fig. 7b) and La Niña (Fig. 7c). Yanase et al. (2012) have shown that shear increases over the southern BoB in the days prior to tropical cyclogenesis indicating that higher shear found during La Niña is favorable for TC development. The enhanced shear during La Niña can act to strengthen convective systems through the tilting and stretching of horizontal vorticity. In the presence of non-uniform rising vertical motion, such as a convective system, and background horizontal vorticity, the horizontal vorticity can be tilted unevenly resulting in the vertical vorticity. This induces additional rising motion stretching the vortex and increases vorticity further. As these systems track into the central BoB where vertical shear is lower, tropical cyclone development can occur. This is limited during El Niño due to the presence of higher shear in the northern BoB. The anomalous wind shear patterns are due to ENSO altered meridional temperature profiles (not shown). During El Niño, temperatures are cooler near the top of the atmosphere at  $20^\circ\text{N/S}$ . This enhances the meridional temperature gradient and strengthens wind shear over the northern BoB by thermal wind arguments. The pattern is reversed during La Niña. Temperatures are warmer and the weakened meridional temperature gradient causes wind shear to weaken over the northern BoB. This favors the



development of tropical systems that track into the northern BoB and explains why more TC formation is favored during La Niña.

Previous research on the role of vertical wind shear over the BoB during the ENSO has yielded conflicting results. Camargo et al. (2007) determined that wind shear was the limiting parameter while GR (2012) noted that shear had a negligible impact on TC formation. Due to the short time scale of TCs, the climatological analysis by the previous authors may not be capturing the variability of wind shear that drives the difference in TC activity between ENSO phases. In order to investigate the impact of ENSO on daily wind shear, a storm relative reference frame is adopted. Shear is averaged zonally over the BoB  $\pm 30$  days relative to storm formation from the equator to  $25^\circ\text{N}$ . The anomalies are determined from the background mean shear (33-year) centered on the mean genesis date (day 314). Both regimes exhibit different patterns prior to genesis (Fig. 8). During La Niña shear increases along the entire southern BoB in the days prior to genesis (Fig. 8b). An examination of the 200 hPa and 850 hPa winds indicates that the increase in shear is primarily due to strengthened 850 hPa zonal winds (not shown). The significantly weaker shear over the northern BoB favors the development and strengthening of TCs as they track northwards. Additionally, the increase in low-level zonal winds provides additional background low-level vorticity for cyclones to develop. The pattern during El Niño is significantly different with weaker shear over the southern BoB (Fig. 8a). The decrease in wind shear over the equatorial region is less favorable for cyclones to form because of less background cyclonic vorticity. Examining the environment around each storm during El Niño, conditions are similar to the background mean with weak anomalies. This indicates that shear is decreasing, relative to Fig. 7a, over the northern BoB prior to genesis allowing for TCs to develop. The number of days when shear is greater than  $20 \text{ m s}^{-1}$  also varies significantly between La Niña (9.1 days) and El Niño (2.6 days) phases ( $p < 0.05$ ,  $t$  test). Positive shear anomalies over the southern BoB serve as a proxy for cyclonic low-level vorticity, which is more conducive for TC formation during La Niña.

Mid-level humidity also plays an important role in the development of tropical systems. Anomalous positive relative humidity pulses have been linked to TC development during October and November over the BoB (Yanase et al. 2012). Li et al. (2013) showed that higher relative humidity from October to November favors more tropical cyclogenesis during these months in comparison to the April to May when relative humidity is lower. Humidity is higher over the BoB at both the 700 hPa (Fig. 9a) and 850 hPa (Fig. 9b.), leading to favorable conditions for enhanced cyclogenesis during La Niña events. To determine the cause of the comparatively higher humidity values during La Niña, vertically integrated moisture transport and precipitable water are examined (Fig. 10). Climatological integrated moisture

transport and precipitable water favor high moisture content over the entire southern BoB (Fig. 10a,b). Wind patterns during El Niño (Fig. 10c) result in weaker moisture transport over the BoB. The weakened jet over the Indo-Chinese peninsula and stronger easterlies along the equator lead to less precipitable water over the BoB (Fig. 10d). Conversely under the La Niña regime (Fig. 10e), westerly winds along the equator and southern BoB transport moisture towards the region. This results in the accumulation of precipitable water (Fig. 10f) over the central and eastern BoB. The additional moisture during La Niña supports enhanced convection and precipitation, shown in Fig. 4, which are important environmental conditions for cyclogenesis to occur. Enhanced moisture also favors latent heat release that is required for TC development and strengthening.

Large absolute vorticity and high relative humidity variability with a periodicity of approximately 30 to 40 days has been linked to tropical cyclone formation over the BoB (Yanase et al. 2012). To further diagnose the impact of relative humidity, a storm relative reference frame is adopted (as in Fig. 8). Patterns during each ENSO phase exhibit distinct evolutions in time (Fig. 11). Enhanced moisture over the southern BoB occurs during both El Niño event (Fig. 11a) and La Niña events (Fig. 11b) 20 to 30 days before genesis. Anomalously dry air is present over the northern BoB in the El Niño composite that is much weaker during La Niña. The presence of drier air over the northern BoB inhibits TC formation during El Niño, while during La Niña, TC activity is distributed over the entire BoB due to comparatively more moisture. These results are consistent with those of Yanase et al. (2012) that TC formation coincides with a northward propagating humidity pulse. The new finding is that a humidity signal appears in both ENSO phases, but TC genesis is favored during La Niña due to enhanced moisture over the entire BoB. This signal could be the result of ENSO altered Madden-Julian Oscillations and should be examined in the future.

Sea surface temperatures (SSTs) have been shown to play a crucial role in the development and strengthening of tropical systems in the BoB (Singh et al. 2001; Yu and McPhaden 2011). SODA SSTAs exhibit differing patterns during El Niño (Fig. 12a) and La Niña (Fig. 12b). Under La Niña conditions, anomalously strong winds force evaporation that cools SSTs, while during El Niño weaker winds allow for SSTs to rise in the southern BoB. The anomalous OLR fields also contribute to the observed temperature differences. Warming or cooling during each ENSO phase in the Indian Ocean is primarily attributed to basin wide surface heat flux anomalies (Hong et al. 2010). Increased wind variability creates a positive feedback cycle between surface winds and convection with enhanced evaporation supporting enhanced atmospheric convection resulting in cooler SSTs. Enhanced (inhibited) convective activity forced by La Niña (El Niño) blocks (allows) solar radiation to reach the ocean

surface resulting in cooling (warming) over the northern BoB. The drop in SSTs is small during La Niña due to enhanced stratification in the upper ocean (Murty et al. 1996, Bhat et al. 2002, Vinayachandran et al. 2002, Sengupta et al. 2008). SSTs are above 28°C during both regimes, well above the tropical cyclone formation threshold value of 26.5°C, and support the findings by GR (2012). Future research will be directed towards determining the exact cause of the differences between SSTAs between ENSO events over the BoB.

## **5. Summary and Discussion**

Post-monsoon season tropical cyclone activity is more favorable during La Niña events over the BoB due to a variety of factors. Previous studies have shown that Niño3.4 SSTAs are correlated with ACE during the post-monsoon season (GR, 2012). We have shown through statistical analyses that La Niña events are correlated with an increase in tropical cyclone activity (ACE) in the BoB at extended lead times (up to 5 months) during the post-monsoon season. This indicates that Niño3.4 SSTAs can be used as a predictor for the upcoming post-monsoon tropical cyclone seasons. An analysis performed for the pre-monsoon season shows no statistical relationship between ACE and Niño3.4 SSTAs over the time period of the study.

Previous research by Camargo et al. (2007) examines TC activity conditions impacted by ENSO globally using Emanuel and Nolan's (2004) Genesis Potential Index (GPI). The analysis was conducted on environmental parameters averaged over a three-month time frame, which coincided with the months prior to peak TC activity over the BoB (August – October). In this study we examined the climatological patterns and daily evolution of the parameters known to impact TC formation during the peak season over the BoB (October – December). The results of Camargo et al. (2007) concluded that lower shear over the BoB during August – October was driving the differences in observed TC activity. Our results show the increase in shear over the equator and decrease over the northern BoB play an important role on modulating TC genesis and intensity during La Niña.

GR (2012) pointed out the important connection between tropical cyclone activity and the ENSO signal and analyzed some environmental conditions. We expand upon these findings and show that the ENSO signal also leads TC activity over the BoB by a period of 5-6 months. The findings of GR (2012) also contradict those of Camargo et al. (2007) concluding that climatological wind shear patterns were similar during both ENSO phases and did not play an important role in modulating TC activity. Our analyses reveal that the increase (decrease) in shear over the southern (northern) BoB during La Niña favors TC development. GR (2012) also did not examine humidity patterns during the ENSO and this is

elaborated in this study. We also work through the synoptic conditions that led to the ENSO altered wind patterns observed over the BoB.

Composites of low-level winds constructed over the BoB for the post-monsoon season (October – December) show cyclonic (anticyclonic) patterns during La Niña (El Niño). This anomalous vorticity is caused by anomalous westerly (easterly) winds that arise as a result of enhanced (suppressed) convective activity over the eastern BoB and Indian Ocean. The large-scale cyclonic rotation provides a favorable environment by supplying additional background vorticity for TC formation. Convective conditions observed during La Niña also create a suitable synoptic pattern for wind bursts to occur due to the increase zonal 10-m wind variance. These wind bursts are important since they help generate low-level cyclonic vorticity, aiding TC development.

La Niña events have enhanced cyclonic vorticity due to favorable atmospheric circulation patterns. During both ENSO phases, climatological vertical wind shear was below  $26 \text{ m s}^{-1}$ , the maximum wind shear during TC genesis. Higher shear over the equatorial and southern BoB aids the development of convective systems during La Niña events. As convective complexes track into the low shear environment in the central BoB TC formation is favored. Relative humidity is also higher over the BoB during La Niña events due to the environmental wind patterns that favor high precipitable water patterns. An examination of humidity patterns leading up to TC formation shows a stronger northward propagating signal during La Niña that favors TC formation. Patterns during El Niño limit the northward progression of the humid air mass due to drier air over the northern BoB that restricts TC development. Future research should investigate if this signal is associated with ENSO altered Madden-Julian Oscillation (MJO) patterns since the periodicity of the humidity signal is within the MJO band (~30 days). SST cooling is the result of increased latent heat flux due to stronger winds and increased cloud cover due to convective activity during La Niña. The cooler SSTs serve as a proxy for increased evaporation aiding convective activity and increasing precipitation seen in the OLR and GPCP composites. Wind patterns favor moisture accumulation over the BoB, which supports the observed enhanced convection during La Niña.

The variation in tropical cyclone activity over the BoB during ENSO events is forced by a combination of factors. La Niña conditions comparatively offer a more favorable environment due to low-level cyclonic vorticity, wind patterns, and increased moisture.

## ***Acknowledgments***

The authors would like to thank the editor and three anonymous reviewers for their constructive comments in the revision of this manuscript. This work was supported by the Office of Naval Research (ONR) Award# N00014-12-1-0454 awarded to BS. One of the authors, VSNM, is thankful to the Director, CSIR-NIO for his keen interest in the joint-collaborative research with BS at the University of South Carolina, Columbia, USA. This has the NIO contribution number XXXX.

## **References**

- Bhat, G. S., and collaborators, 2001: BOMEX: The Bay of Bengal monsoon experiment, *Bull. Amer. Meteorol. Soc.*, **82**, 2217–2243.
- Bjerknes, J., 1969: Atmospheric Teleconnections from the Equatorial Pacific. *Mon. Wea. Rev.*, **97**, 63–172.
- Bolton, D., 1980: The Computation of Equivalent Potential Temperature. *Mon. Wea. Rev.*, **108**, 1046–1053.
- Camargo, S. J., K. A. Emanuel and A. H. Sobel, 2007: Use of a Genesis Potential Index to Diagnose ENSO Effects on Tropical Cyclone Genesis. *J. Climate*, **20**, 4819–4834.
- Emanuel, K. A. and D. S. Nolan, 2004: Tropical cyclone activity and global climate, Preprints, *26th Conf. on Hurricanes and Tropical Meteorology*, Miami, FL, Amer. Meteor. Soc., 240–241.
- Giese, B. S., and S. Ray, 2011: El Niño variability in simple ocean data assimilation (SODA), 1871–2008, *J. Geophys. Res.*, **116**, C02024, doi:10.1029/2010JC006695.
- Girishkumar, M. S. and M. Ravichandran, 2012: The influences of ENSO on tropical cyclone activity in the Bay of Bengal during October-December. *Geophys. Res. Lett.*, **117**, C02033.
- Goswami, B. N., R. S. Ajayamohan, P. K. Xavier, and D. Sengupta, 2003: Clustering of synoptic activity by Indian summer monsoon intraseasonal oscillations. *Geophys. Res. Lett.*, **30(8)**, 1431.
- Gray, W. M., 1968: Global View of the Origin of Tropical Disturbances and Storms. *Mon. Wea. Rev.*, **96**, 669–700.
- Gray, W.M., 1998: The Formation of Tropical Cyclones. *Meteor. Atmos. Phys.*, **67**, 37-69.
- Hong, C., T. Li, LinHo and Y. Chen, 2010: Asymmetry of the Indian Ocean Basinwide SST Anomalies: Roles of ENSO and IOD\*. *J. Climate*, **23**, 3563–3576.
- Kanamitsu, M., W. Ebisuzaki, J. Woollen, S-K. Yang, J. J. Hnilo, M. Fiorino and G. L. Potter, 2002: NCEP–DOE AMIP-II Reanalysis (R-2). *Bull. Amer. Meteor. Soc.*, **83**, 1631–1643.
- Kikuchi, K., B. Wang, and H. Fudeyasu, 2009: Genesis of tropical cyclone Nargis revealed by multiple satellite observations, *Geophys. Res. Lett.*, **36**, L06811.
- Kikuchi, K. and B. Wang, 2010: Formation of Tropical Cyclones in the Northern Indian Ocean Associated with Two Types of Tropical Intraseasonal Oscillation Modes. *J. Meteor. Soc. Japan.*, **88(3)**, 475–496.

- Kurihara, Y., M. A. Bender, R. E. Tuleya, R. J. Ross, 1990: Prediction Experiments of Hurricane Gloria (1985) Using a Multiply Nested Movable Mesh Model. *Mon. Wea. Rev.*, **118**, 2185–2198.
- Li, K., W. Yu, T. Li, V. S. N. Murty, S. Khokiattiwong, T. R. Adi, and S. Budi, 2013: Structures and mechanisms of the first-branch northward-propagating intraseasonal oscillation over the tropical Indian Ocean. *Climate Dyn.*, **40**, 1707-1720.
- Li, Z., W. Yu, T. Li, V. S. N. Murty, F. Tangang, 2013: Bimodal Character of Cyclone Climatology in the Bay of Bengal Modulated by Monsoon Seasonal Cycle\*. *J. Climate*, **26**, 1033–1046.
- Lin, I. I., C. H. Chen, I. F. Pun, W. T. Liu and C. C. Wu, 2009: Warm ocean anomaly, air sea fluxes, and the rapid intensification of tropical cyclone Nargis (2008), *Geophys. Res. Lett.*, **36**, L03817.
- Maneesha, K., V. S. N. Murty, M. Ravichandran, T. Lee, W. Yu and M. J. McPhaden, 2012: Upper ocean variability in the Bay of Bengal during the tropical cyclones Nargis and Laila, *Prog. Oceanogr.*, **106**, 49-61.
- McPhaden, M. J., G. R. Foltz, T. Lee, V. S. N. Murty, M. Ravichandran, G. A. Vecchi, J. Vialard, J. D. Wiggert and L. Yu, 2009: Ocean-Atmosphere Interactions During Cyclone Nargis. *EOS Trans. AGU.*, **90(7)**, 53–60.
- Murty, V. S. N., Y. V. B. Sarma, and D. P. Rao, 1996: Variability of the oceanic boundary layer characteristics in the northern Bay of Bengal during MONTBLEX-90, *Earth Planet Sci.*, **105**, 41–61.
- Sengupta, D., B. R. Goddalahundi, and D. S. Anitha, 2008: Cyclone-induced mixing does not cool SST in the post-monsoon north Bay of Bengal. *Atmos. Sci. Lett.*, **9**, 1–6. doi: 10.1002/asl.162.
- Singh, O. P., T. M. Ali Khan and Md. S. Rahman, 2000: Changes in the frequency of TCs over the North Indian Ocean. *Meteor. Atmos. Phys.*, **75**, 11–20.
- Singh, O. P., T. M. Ali Khan and Md. S. Rahman, 2001: Probable reasons for enhanced cyclogenesis in the Bay of Bengal during July-August of ENSO years. *Global Planet. Change.*, **29**, 135–147.
- Smith, R. D., J. K. Dukowicz and R. C. Malone, 1994: Parallel ocean general circulation modeling, *Physica D: Nonlinear Phenomena*, **60**, 38-61.
- Trenberth, K. E., 1997: The Definition of El Niño. *Bull. Amer. Meteor. Soc.*, **78**, 2771–2777.
- Vinayachandran, P. N., V. S. N. Murty, and V. Ramesh Babu, 2002: Observations of barrier layer formation in the Bay of Bengal during summer monsoon, *J. Geophys. Res.*, **107** (C12), 8018, doi:10.1029/2001JC000831.
- Yanase, W., M. Satoh, H. Taniguchi and H. Fujinami, 2012: Seasonal and Intraseasonal Modulation of Tropical Cyclogenesis Environment over the Bay of Bengal during the Extended Summer Monsoon. *J. Climate*, **25**, 2914–2930.
- Yu, L. and M. J. McPhaden, 2011: Ocean Preconditioning of Cyclone Nargis in the Bay of Bengal: Interaction between Rossby Waves, Surface Fresh Waters, and Sea Surface Temperatures. *J. Phys. Oceanogr.*, **41**, 1741–1755.

### *List of Tables*

TABLE 1. Occurrences and frequencies of the tropical systems (cyclones and depressions) during the post-monsoon season (October – December) over the Bay of Bengal for ENSO events. The number of tropical systems that comprise the total and did not reach a minimum wind speed of 35 knots during its lifetime are shown in parentheses.

TABLE 2. Correlation coefficients between monthly Niño3.4 SSTAs and ACE totals from October – December (1979-2011). Italicized (bolded) values signify correlations where  $p$ -values < 0.05 (0.01).

TABLE 3. Same as Table 2, except for the months of March through May (1979-2011). Negative values (-1) next to month names indicate Niño3.4 SSTAs taken from the previous year while zeros (0) are from the concurrent year of the ACE totals. No correlations have  $p$ -values < 0.05.

## *List of Figures*

FIG. 1. Seasonal distribution of tropical systems and ACE ( $\text{kt}^2$ ) in the Bay of Bengal over the study period of 1979-2011. ACE is scaled by a factor of  $\frac{1}{4}$  for ease of comparison. The white numbers in each column represent the number of tropical systems that formed during each month without attaining the threshold value of 35 knots during its lifetime over the 33-year time period.

FIG. 2. Post-monsoon season (October- December) tropical cyclone genesis and tracks during (a) El Niño and (b) La Niña events over the period of 1979-2011 in the Bay of Bengal. Red plus signs (blue solid lines) indicate genesis locations (track) for storms that reached a minimum wind speed of 35 knots over its lifetime. Black stars (dashed blue lines) indicate genesis locations (tracks) for storms that did not reach a minimum speed of 35 knots.

FIG. 3. Pre-monsoon season (March - May) tropical cyclone genesis locations and tracks in the Bay of Bengal over the period of 1979-2011. Red plus signs (blue solid lines) indicate genesis locations (track) for storms that reached a minimum wind speed of 35 knots over its lifetime. Black stars (dashed blue lines) indicate genesis locations (tracks) for storms that did not reach a minimum speed of 35 knots.

FIG. 4. (Top Shaded) Post-monsoon season (October-December) averaged 925 hPa wind magnitude ( $\text{m s}^{-1}$ ) composites during (a) El Niño events and (b) La Niña events. (Top) Vectors represent wind anomalies during each ENSO phase where  $p < 0.1$  using a Student's  $t$  test relative to the 33-year mean. (Bottom) Same as top, but for 925 hPa relative vorticity anomalies ( $\text{s}^{-1}$ ) during (c) El Niño events and (d) La Niña events. Positive (negative) values correspond to anomalous cyclonic (anti-cyclonic) vorticity.

FIG. 5. Difference in post-monsoon season (a) OLR ( $\text{W m}^{-2}$ ) and (b) GPCP precipitation anomalies ( $\text{mm day}^{-1}$ ) between La Niña and El Niño. Regions enclosed by contouring represent differences in the anomalies between El Niño and La Niña at  $p < 0.1$  using a Student's  $t$  test. Negative OLR values correspond indicate stronger convection during La Niña while positive precipitation values indicate higher precipitation during La Niña.

FIG. 6. Difference of 10-meter zonal wind standard deviation between La Niña and El Niño. Regions enclosed by contouring represent differences in the anomalies between each El Niño and La Niña at  $p < 0.1$  using a Student's  $t$  test. Positive (negative) values indicate greater variance during La Niña (El Niño).

FIG. 7. Post-monsoon season 200–850 hPa vertical wind shear ( $\text{m s}^{-1}$ ) for (a) the 33-year mean, (b) anomalies during El Niño, and (c) anomalies during La Niña events. Regions enclosed by



contouring represent differences in the anomalies between each ENSO phase and the 33-year mean at  $p < 0.1$  using a Student's  $t$  test.

FIG. 8. Time-latitude composite diagrams of deep layer wind shear (200-850 hPa) anomalies ( $\text{m s}^{-1}$ ) during (a) El Niño and (b) La Niña events spanning a 60 day period relative to TC formation ( $\pm 30$  days). The anomalies are based of the 33-year mean centered on the mean genesis date (day 314). The values for each point represent wind shear magnitude averaged every  $2.5^\circ$  of latitude between  $80^\circ\text{E}$  and  $100^\circ\text{E}$ . The genesis latitude of each storm is marked with an open circle. Day zero is reference to when the tropical cyclone first reached wind speeds of 20 kt (weak depression). Regions enclosed by contouring represent differences in the anomalies between (a) El Niño and (b) La Niña and the 33-year mean at  $p < 0.1$  using a Student's  $t$  test.

FIG. 9. Difference (La Niña minus El Niño) between (a) 700 hPa and (b) 850 hPa post-monsoon season averaged relative humidity (%). Positive (negative) values represent higher values in the La Niña (El Niño) composites. Regions enclosed by contouring represent differences in the anomalies between each ENSO phase at  $p < 0.1$  using a Student's  $t$  test.

FIG. 10. (Left: a,c,e) Vertically integrated moisture transport,  $\mathbf{Q}$ , and vectors for (a) the 33-year mean, (c) anomalies during El Niño, and (e) anomalies during La Niña ( $\text{kg m}^{-1} \text{s}^{-1}$ ). (Right: b,d,f) Same as left, except for precipitable water,  $W$  ( $\text{kg m}^{-2}$ ). Regions enclosed by contouring represent El Niño (c,d) and La Niña (e,f) anomalies that vary significantly from the 33-year mean ( $p$  value  $< 0.1$ , Student's  $t$  test).

FIG. 11. Time-latitude composite diagrams of 600 hPa relative humidity anomalies (%) during (a) El Niño and (b) La Niña events spanning a 60 day period relative to TC formation ( $\pm 30$  days). The anomalies are based of the 33-year mean centered on the mean genesis date (day 314). The values for each point represent the humidity averaged every  $2.5^\circ$  of latitude between  $80^\circ\text{E}$  and  $100^\circ\text{E}$ . The genesis latitude of each storm is marked with an open circle. Day zero is reference to when the tropical cyclone reached wind speeds of 20 kts (weak depression). Regions enclosed by contouring represent differences in the anomalies between (a) El Niño and (b) La Niña and the 33-year mean at  $p < 0.1$  using a Student's  $t$  test.

FIG. 12. SODA SSTAs ( $^\circ\text{C}$ ) composites for (a) El Niño and (b) La Niña events. Warm (cool) regions indicate higher (lower) SSTAs during each respective ENSO phase. SSTs during El Niño and La Niña are contoured at  $0.5^\circ\text{C}$  interval.

TABLE 1. Occurrences and frequencies of the tropical systems (cyclones and depressions) during the post-monsoon season (October – December) over the Bay of Bengal for ENSO events. The number of tropical systems that comprise the total and did not reach a minimum wind speed of 35 knots during its lifetime are shown in parentheses.

ENSO Cycle	Number of Years	Number of Tropical Systems	Tropical Systems per Year
El Niño	10	16 (2)	1.60
Neutral	12	27 (6)	2.25
La Niña	11	31	2.82

TABLE 2. Correlation coefficients between monthly Niño3.4 SSTAs and ACE totals from October – December (1979-2011). Italicized (bolded) values signify correlations where  $p$ -values < 0.05 (0.01).

Month	Correlation Coefficients
Jan	-0.02
Feb	-0.05
Mar	-0.11
Apr	-0.24
May	-0.38
Jun	<b>-0.50</b>
Jul	<b>-0.56</b>
Aug	<b>-0.58</b>
Sep	<b>-0.60</b>
Oct	<b>-0.62</b>
Nov	<b>-0.64</b>
Dec	<b>-0.66</b>

TABLE 3. Same as Table 2, except for the months of March through May (1979-2011). Negative values (-1) next to month names indicate Niño3.4 SSTAs taken from the previous year while zeros (0) are from the concurrent year of the ACE totals. No correlations have  $p$ -values < 0.05.

Month	Correlation Coefficients
Jun (-1)	-0.12
Jul (-1)	-0.08
Aug (-1)	-0.06
Sep (-1)	-0.06
Oct (-1)	-0.07
Nov (-1)	-0.07
Dec (-1)	-0.06
Jan (0)	-0.05
Feb (0)	-0.03
Mar (0)	0.00
Apr (0)	0.09
May (0)	0.21

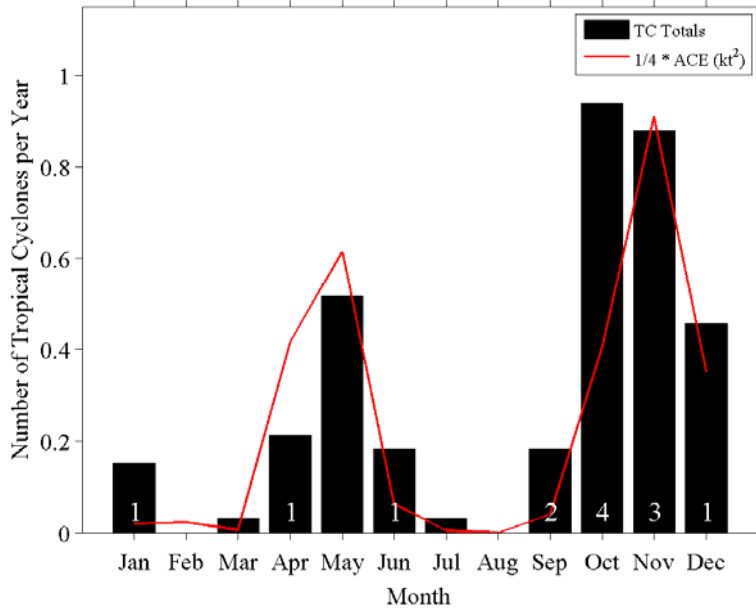


FIG. 1. Seasonal distribution of tropical systems and ACE ( $\text{kt}^2$ ) in the Bay of Bengal over the study period of 1979-2011. ACE is scaled by a factor of  $\frac{1}{4}$  for ease of comparison. The white numbers in each column represent the number of tropical systems that formed during each month without attaining the threshold value of 35 knots during its lifetime over the 33-year time period.

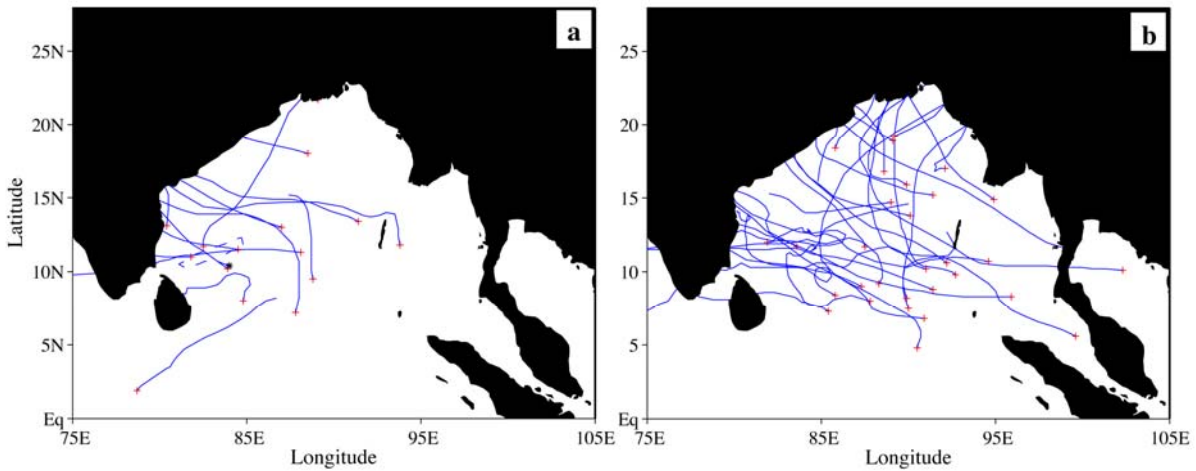


FIG. 2. Post-monsoon season (October- December) tropical cyclone genesis and tracks during (a) El Niño and (b) La Niña events over the period of 1979-2011 in the Bay of Bengal. Red plus signs (blue solid lines) indicate genesis locations (track) for storms that reached a minimum wind speed of 35 knots over its lifetime. Black stars (dashed blue lines) indicate genesis locations (tracks) for storms that did not reach a minimum speed of 35 knots.

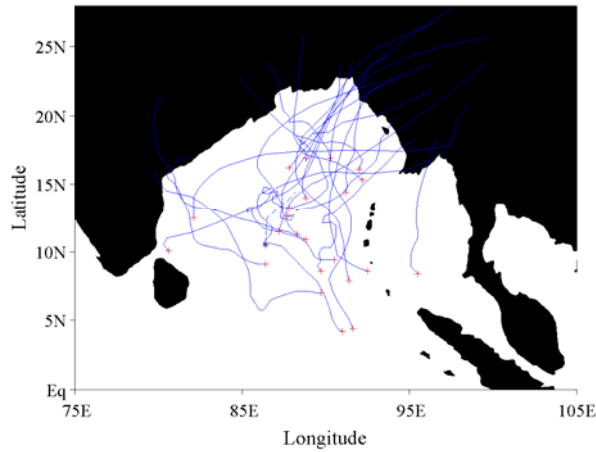


FIG. 3. Pre-monsoon season (March - May) tropical cyclone genesis locations and tracks in the Bay of Bengal over the period of 1979-2011. Red plus signs (blue solid lines) indicate genesis locations (track) for storms that reached a minimum wind speed of 35 knots over its lifetime. Black stars (dashed blue lines) indicate genesis locations (tracks) for storms that did not reach a minimum speed of 35 knots.

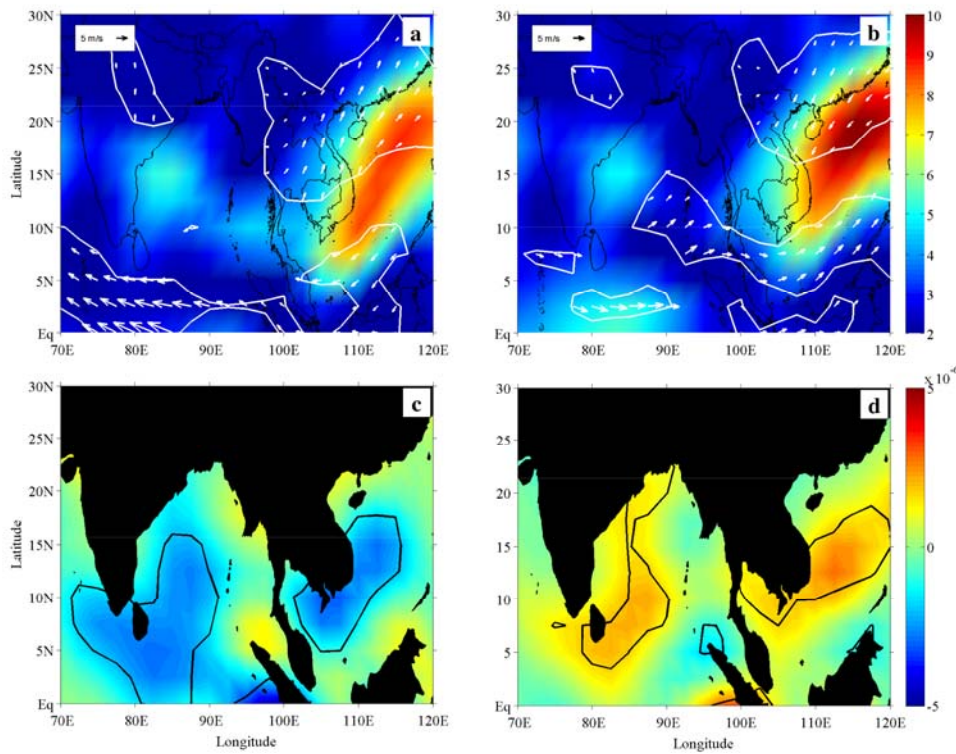


FIG. 4. (Top Shaded) Post-monsoon season (October-December) averaged 925 hPa wind magnitude ( $\text{m s}^{-1}$ ) composites during (a) El Niño events and (b) La Niña events. (Top) Vectors represent wind anomalies during each ENSO phase where  $p < 0.1$  using a Student's  $t$  test relative to the 33-year mean. (Bottom) Same as top, but for 925 hPa relative vorticity anomalies ( $\text{s}^{-1}$ ) during (c) El Niño events and (d) La Niña events. Positive (negative) values correspond to anomalous cyclonic (anti-cyclonic) vorticity.

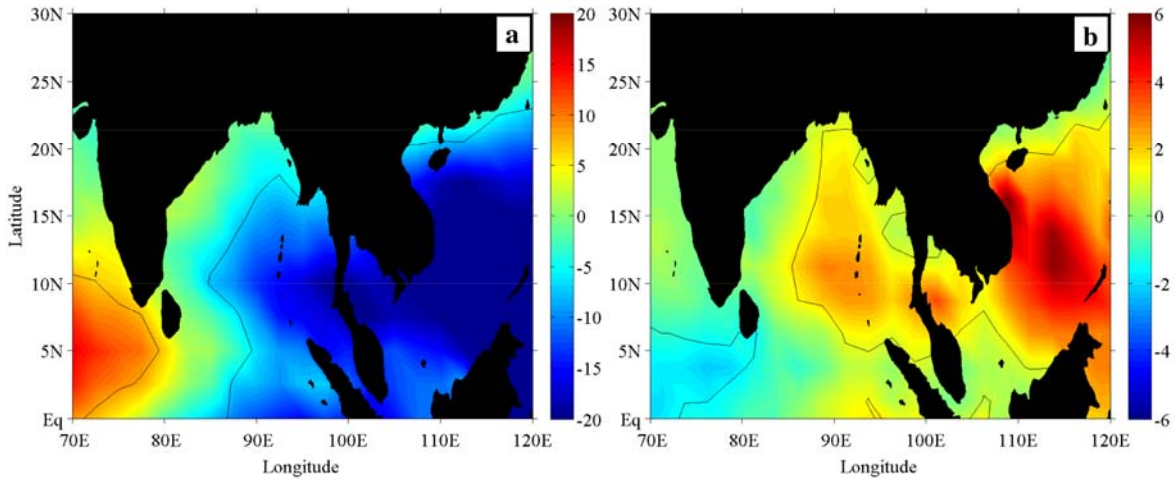


FIG. 5. Difference in post-monsoon season (a) OLR ( $\text{W m}^{-2}$ ) and (b) GPCP precipitation anomalies ( $\text{mm day}^{-1}$ ) between La Niña and El Niño. Regions enclosed by contouring represent differences in the anomalies between El Niño and La Niña at  $p < 0.1$  using a Student's  $t$  test. Negative OLR values indicate stronger convection during La Niña while positive precipitation values indicate higher precipitation during La Niña.

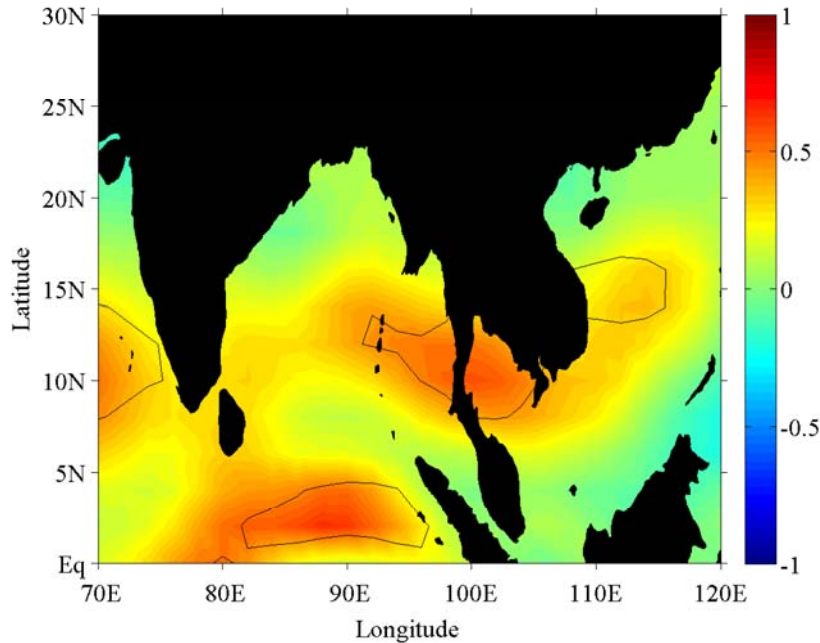


FIG. 6. Difference of 10-meter zonal wind standard deviation between La Niña and El Niño. Regions enclosed by contouring represent differences in the anomalies between each El Niño and La Niña at  $p < 0.1$  using a Student's  $t$  test. Positive (negative) values indicate greater variance during La Niña (El Niño).

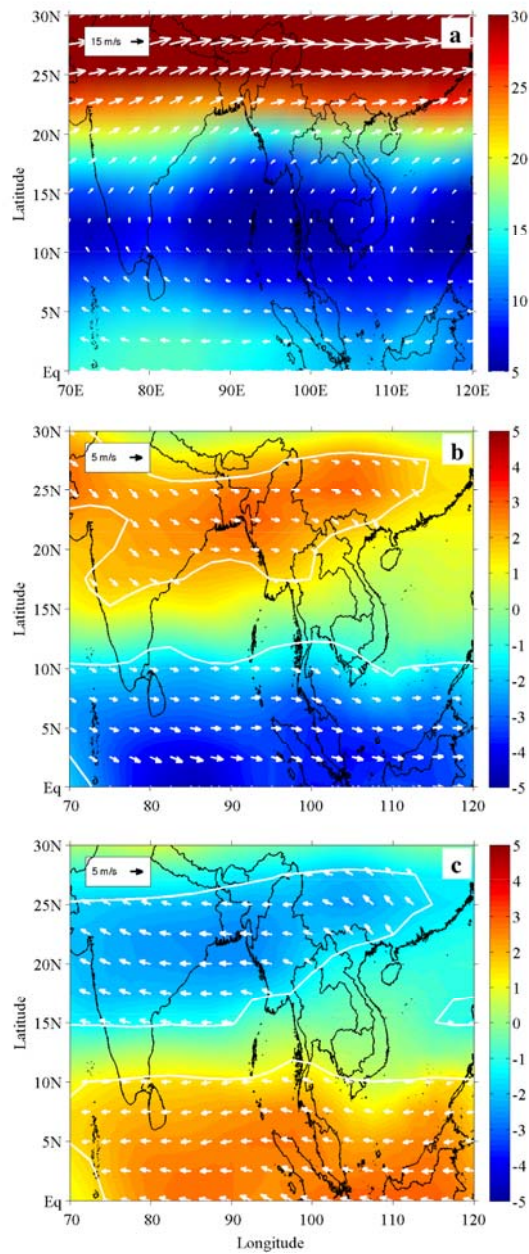


FIG. 7. Post-monsoon season 200–850 hPa vertical wind shear ( $\text{m s}^{-1}$ ) for (a) the 33-year mean, (b) anomalies during El Niño, and (c) anomalies during La Niña events. Regions enclosed by contouring represent differences in the anomalies between each ENSO phase and the 33-year mean at  $p < 0.1$  using a Student's  $t$  test.

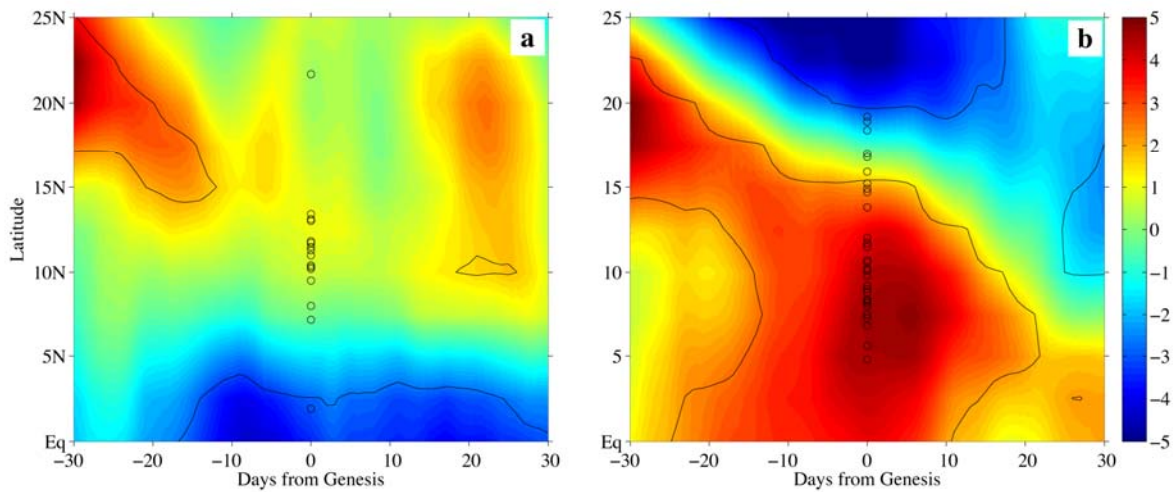


FIG. 8. Time-latitude composite diagrams of deep layer wind shear (200-850 hPa) anomalies ( $\text{m s}^{-1}$ ) during (a) El Niño and (b) La Niña events spanning a 60 day period relative to TC formation ( $\pm 30$  days). The anomalies are based on the 33-year mean centered on the mean genesis date (day 314). The values for each point represent wind shear magnitude averaged every  $2.5^\circ$  of latitude between  $80^\circ\text{E}$  and  $100^\circ\text{E}$ . The genesis latitude of each storm is marked with an open circle. Day zero is reference to when the tropical cyclone first reached wind speeds of 20 kt (weak depression). Regions enclosed by contouring represent differences in the anomalies between (a) El Niño and (b) La Niña and the 33-year mean at  $p < 0.1$  using a Student's  $t$  test.

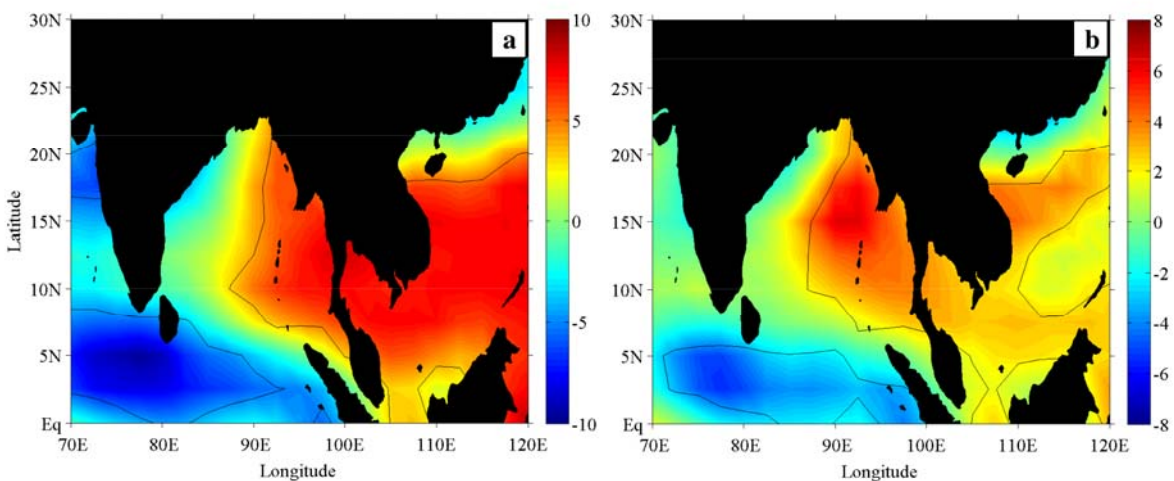


FIG. 9. Difference (La Niña minus El Niño) between (a) 700 hPa and (b) 850 hPa post-monsoon season averaged relative humidity (%). Positive (negative) values represent higher values in the La Niña (El Niño) composites. Regions enclosed by contouring represent differences in the anomalies between each ENSO phase at  $p < 0.1$  using a Student's  $t$  test.

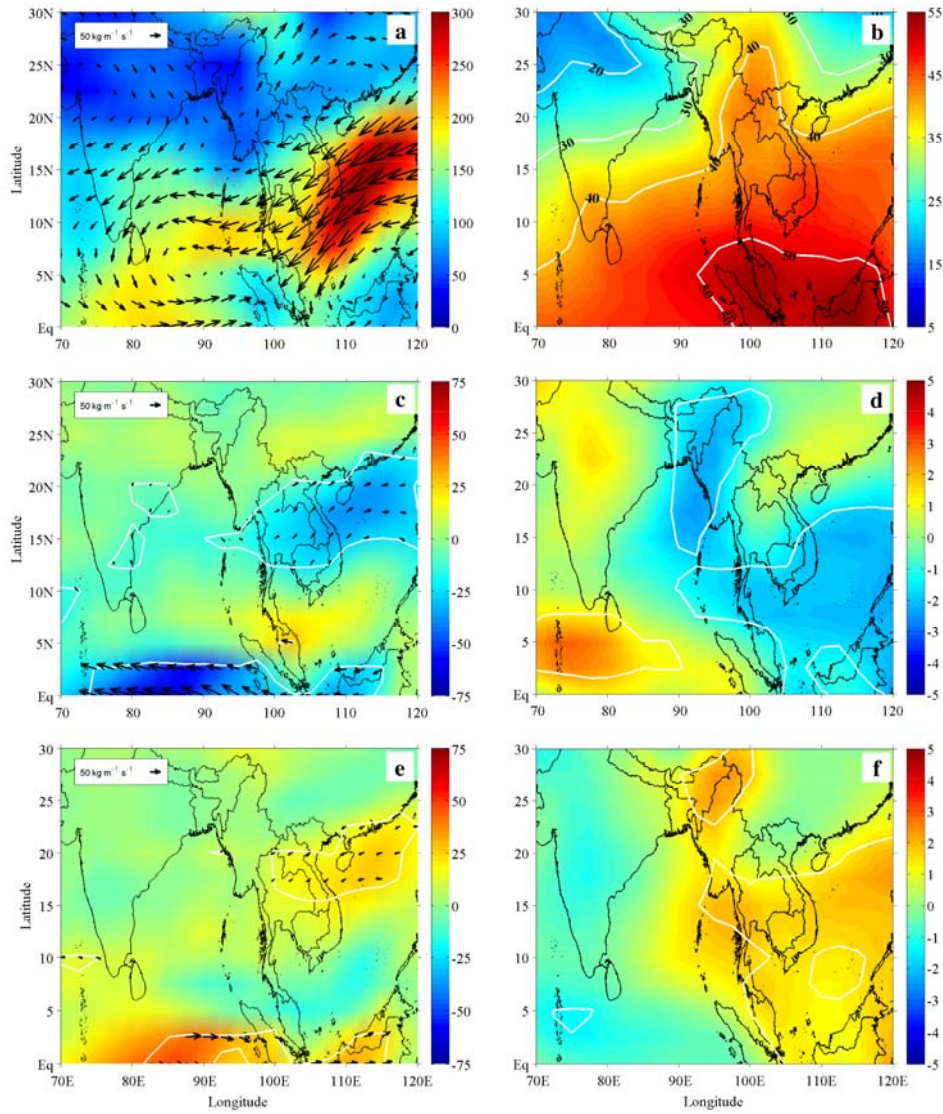


FIG. 10. (Left: a,c,e) Vertically integrated moisture transport,  $\mathbf{Q}$ , and vectors for (a) the 33-year mean, (c) anomalies during El Niño, and (e) anomalies during La Niña ( $\text{kg m}^{-1} \text{ s}^{-1}$ ). (Right: b,d,f) Same as left, except for precipitable water,  $W$  ( $\text{kg m}^{-2}$ ). Regions enclosed by contouring represent El Niño (c,d) and La Niña (e,f) anomalies that vary significantly from the 33-year mean ( $p$  value  $< 0.1$ , Student's  $t$  test).



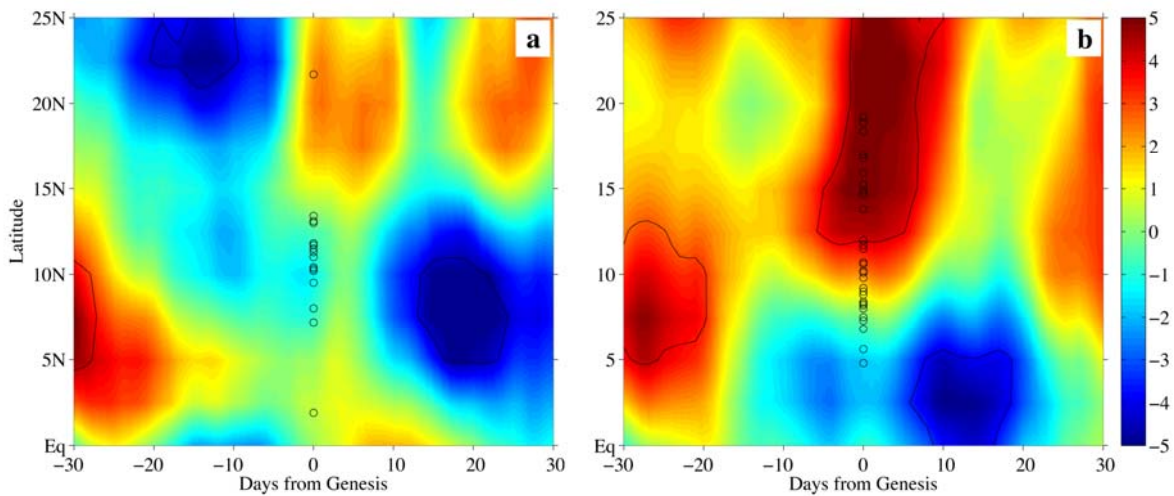


FIG. 11. Time-latitude composite diagrams of 600 hPa relative humidity anomalies (%) during (a) El Niño and (b) La Niña events spanning a 60 day period relative to TC formation ( $\pm 30$  days). The anomalies are based on the 33-year mean centered on the mean genesis date (day 314). The values for each point represent the humidity averaged every  $2.5^\circ$  of latitude between  $80^\circ\text{E}$  and  $100^\circ\text{E}$ . The genesis latitude of each storm is marked with an open circle. Day zero is reference to when the tropical cyclone reached wind speeds of 20 kts (weak depression). Regions enclosed by contouring represent differences in the anomalies between (a) El Niño and (b) La Niña and the 33-year mean at  $p < 0.1$  using a Student's  $t$  test.

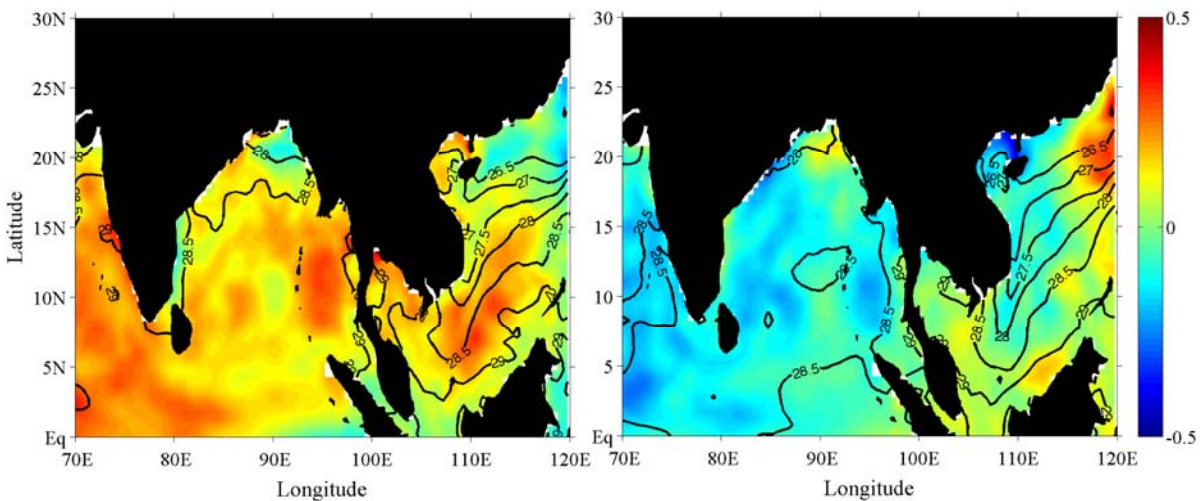


FIG. 12. SODA SSTAs ( $^\circ\text{C}$ ) composites for (a) El Niño and (b) La Niña events. Warm (cool) regions indicate higher (lower) SSTAs during each respective ENSO phase. SSTs during El Niño and La Niña are contoured at  $0.5^\circ\text{C}$  interval.